

The thermo-mechanical state of the Andes in the Altiplano-Puna region: insights from Curie isotherm and effective elastic thickness determination

Federico IBARRA^{1,2} y Claudia B. PREZZI¹

¹CONICET-Universidad de Buenos Aires, Instituto de Geociencias Básicas, Aplicadas y Ambientales de Buenos Aires (IGeBA), Ciudad Autónoma de Buenos Aires.

² Institute of Geosciences, Potsdam University, Potsdam, Germany

Email: ibarra@gl.fcen.uba.ar

Editores invitados: Mariano Larrovere, Pablo Alasino y Sebastián Rocher

ABSTRACT

We present new constraints on the temperature distribution beneath the Altiplano-Puna plateau region and a new model of effective elastic thickness for the Central Andes. The aim of this study is to better assess the thermal state of the plateau and surrounding regions and analyze its influence on the elastic thickness and strength of the lithosphere. We performed a statistical analysis of the magnetic anomaly in frequency domain in order to obtain the depth to the bottom of the magnetic layer, interpreted as the Curie isotherm. The effective elastic thickness was calculated from the flexure analysis in frequency domain of the deflection of the crust and the pseudo-topography (an artificial construction that allows accounting for the internal loads). We find that the Puna and the volcanic arc present the shallowest Curie isotherm and highest heat-flow in agreement with conductivity, velocity and attenuation anomalies suggesting the presence of partial melts within the crust. In addition, the Altiplano exhibits a deeper Curie isotherm in coincidence with other observations pointing to a stronger lithosphere than in the Puna. Our results show that the effective elastic thickness correlates only partially with the thermal state and that, consequently, other processes, such as inheritance of the elastic thickness, need to be considered to explain the observations and avoid misinterpretations in the variability of the thermal field.

Keywords: *Central Andes, Curie point depth, flexural rigidity, lithosphere.*

RESUMEN

El estado termo-mecánico de los Andes en la región del Altiplano-Puna a partir del cálculo de la profundidad de Curie y el espesor elástico

Presentamos nuevos resultados de la distribución de temperatura en la corteza en la región del Altiplano-Puna y un nuevo modelo de espesor elástico para los Andes Centrales. El objetivo de este trabajo es determinar el estado térmico del plateau y alrededores, y analizar su influencia en el espesor elástico y la resistencia a la deformación de la litósfera. Realizamos un análisis estadístico de la anomalía magnética en dominio de frecuencias para obtener la profundidad a la base de la capa magnética, interpretada como la isoterma de Curie. El espesor elástico fue calculado a partir del análisis flexural de la deflexión de la corteza y la pseudo-topografía (construcción artificial que permite incluir las cargas internas) en el dominio de frecuencias. Hallamos que las profundidades más someras de la isoterma de Curie y los valores más altos de flujo térmico se encuentran debajo de la Puna y el arco volcánico, en coincidencia con anomalías de conductividad, velocidad y atenuación sísmica que sugieren la presencia de fundidos en la corteza. Además, observamos que el Altiplano exhibe una isoterma de Curie más profunda coincidente con otras observaciones que apuntan a una litósfera más resistente que la de la Puna. Nuestros resultados muestran que el espesor elástico se correlaciona solo parcialmente con el estado térmico y que en consecuencia, otros procesos tales como herencia del espesor elástico deben ser considerados a la hora de explicar los resultados para así evitar interpretaciones erróneas acerca de la variabilidad del campo termal..

Palabras clave: *Andes Centrales, punto de Curie, rigidez flexural, litósfera*

INTRODUCTION

The Altiplano-Puna plateau in the Central Andes spans ~2000 km in N-S direction and ~300 km from west to east with an average elevation of 3700 m, thus becoming the largest plateau developed in a subduction system and the second largest in the world after Tibet (Fig. 1; Allmendinger *et al.* 1997, Lamb 2000). At the latitudes of the plateau, approximately -15° to -28° , the Nazca plate steeply subducts beneath the South American plate with an average angle of 30° , whereas to the north and south, the plateau is bounded by two flat subduction segments (Isacks 1988, Jordan *et al.* 1983).

The existence of thermal anomalies in the crust and mantle beneath the plateau has been established by a wide variety of independent geological, geochemical and geophysical studies (*e.g.*, Bianchi *et al.* 2013, Koulakov *et al.* 2006, Schurr *et al.* 2003, Springer 1999, Whitman *et al.* 1996). The region is characterized by the presence of large ignimbritic deposits with major crustal contribution and isolated volumetrically small mantle-derived basaltic rocks erupted since Oligo-Miocene times (Fig. 1; *e.g.*, Guzmán *et al.* 2014, Kay *et al.* 1994, Kay *et al.* 2010, Risse *et al.* 2013). Moreover, there are regions in the subsurface with abnormally low seismic velocities, high seismic attenuation and high conductivity located in the upper and middle crust beneath the Southern Puna and the transition between the Altiplano and the Northern Puna (Fig. 1; *e.g.*, Bianchi *et al.* 2013, Chmielowski *et al.* 1999, Whitman *et al.* 1996, Wölbern *et al.* 2009, Yuan *et al.* 2000). In addition, the surface heat-flow throughout the plateau is extremely high (*e.g.*, Hamza and Muñoz 1996, Henry and Pollack 1988, Springer and Förster 1998). Although the extent of the thermal anomaly has been largely constrained, there are only few estimates on the temperature distribution with depth. Kay *et al.* (2010) presented a compilation of regional geochemistry of the ignimbrites in the Puna plateau; pre-eruptive conditions for the younger deposits (up to 2.5 Ma) are estimated to be in the range $770\text{--}840^{\circ}\text{C}$ at 4–8 km depths. Burns *et al.* (2015) showed that in the young Purico-Chascón volcanic complex (~1 Ma) temperatures calculated

with geothermometers lie within a similar range, $790\text{--}890^{\circ}\text{C}$, for depths between 4 km to 8 km. In the same volcanic complex, Schmitt *et al.* (2001) recognized a deeper source working as a recharge area at ~17–20 km with temperatures up to 965°C . From numerical models, Babeyko *et al.* (2002) suggested that temperatures of at least $700\text{--}800^{\circ}\text{C}$ in the middle crust are required to account for magma production. These authors also proposed that the crust was thermally weakened before the generation of the large magma reservoirs in the upper and middle crust.

Determination of the temperature distribution is important because it plays a key role in several lithospheric processes such as isostasy and deformation. Prezzi *et al.* (2014) showed how variations in the thermal state throughout the Altiplano-Puna correlate with different isostatic compensation mechanisms. Ouimet and Cook (2010) suggested that high temperature in the Andean lower crust favored crustal flow and that this mechanism explains recent crustal thickening and generation of topography. Additionally, the effective elastic thickness is intimately related to the thermal state of the lithosphere, although other elements such as coupling state of crust and mantle also have an influence (Burov and Diament 1995, Watts and Burov 2003).

Previous studies have investigated the temperature distribution and effective elastic thickness in the region. Prezzi and Ibarra (2017) calculated the depth to the Curie isotherm and found a link between their results, the thermal anomalies in the crust and the elevated surface heat-flow. Recently, García *et al.* (2018) modelled the effective elastic thickness of the lithosphere and compared it with previous estimates. Their results are similar to those of Watts *et al.* (1995) suggesting a correlation between elastic thickness and deformation style in the foreland, in disagreement with other recent studies (*e.g.*; Stewart and Watts 1997, Tassara 2005, Mantovani *et al.* 2005, Wienecke *et al.* 2007, Pérez-Gussinyé *et al.* 2009).

In this study, we complement the temperature estimates for the Altiplano-Puna region from the statistical analysis of the magnetic anomaly in frequency domain with new calculations of the effective elastic thickness in the Central Andes consid-

ering internal loads and a seismic Moho, in order to analyze the relation between the thermal and mechanical state of the region and the active deformation.

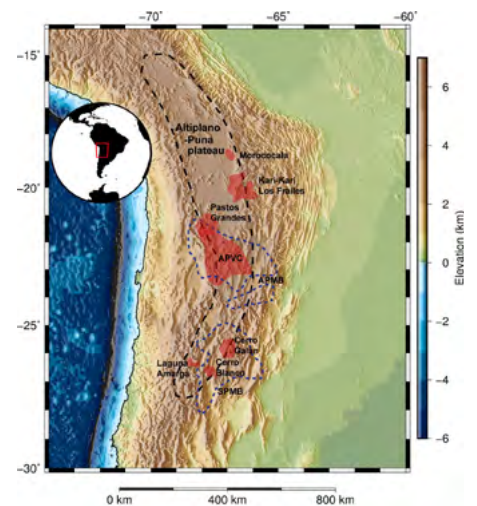


Figure 1. Topographic map of South America showing the location of the Altiplano-Puna plateau (stippled black line), the geophysical anomalies APMB and SPMB (Altiplano-Puna Magma Body and Southern Puna Magma Body; blue stippled lines) and main ignimbritic deposits (red shaded regions). APVC: Altiplano-Puna Volcanic Complex.

GEOLOGIC SETTING

The Altiplano-Puna plateau is a wide internally drained, intraorogenic basin developed on late Neoproterozoic to Paleozoic igneous-metamorphic basement rocks and filled with Cenozoic sedimentary rocks, evaporites and volcanics reaching thicknesses greater than 6 km (Alonso *et al.* 1991, Siks and Horton 2011). An ignimbrite “flare-up” occurred during the Miocene and since then, local volcanic edifices and calderas have evolved within the plateau (*e.g.*, Coira and Kay 1993, Guzmán *et al.* 2014, Kay *et al.* 1994, Viramonte *et al.* 1984). The largest concentration of ignimbrites is located between -21° and -24° ; the region is known as the Altiplano-Puna Volcanic Complex (APVC; de Silva 1989) and extends approximately for 60000 km² with an estimated volume of >15000 km³ (Fig. 1; Burns *et al.* 2015, Guzmán *et al.* 2014). The largest centers north of -21° are the Morococala and Kari-Kari-Los Frailes ignimbrite complexes; south of -24° , the Aguas Calientes, Cerro Galán, Laguna Amarga and Cerro Blanco complexes are the largest outcropping ignimbrites (Fig. 1; Kay *et al.* 2010).

Two main geophysical anomalies have been defined within the crust beneath the plateau. These anomalies are commonly referred to in the literature as low velocity zones or high conductivity zones. From receiver function analysis, Chmielowski *et al.* (1999) identified a prominent thin low-velocity layer at 19 km ($V_s < 0.5$ km/s) between -20° to -23° , interpreted as a regional sill-like magma body associated with the Altiplano-Puna Volcanic Complex as a possible source or reservoir of magmas. They referred to this layer as the Altiplano-Puna Magma Body (Fig. 1). Yuan *et al.* (2000) showed that the Altiplano-Puna Magma Body was larger and thicker than previously imaged, involving most of the middle crust as a region undergoing metamorphism and partial melting. Magnetotelluric and geomagnetic deep soundings in the region revealed the presence of zones with high conductivity (> 10000 S) in the crust of the southern Altiplano and northern Puna between 20–40 km supporting the presence of melt (*e.g.*, Brasse *et al.* 2002, Schwarz *et al.* 1994).

Several studies have investigated the seismic and electrical structure of the crust, improving the definition of the anomaly and identifying areas with low resistivity and high V_p/V_s ratio and attenuation (*e.g.*, Beck and Zandt 2002, Comeau *et al.* 2015, Comeau *et al.* 2016, Díaz *et al.* 2012, Schurr *et al.* 2003, Wölbern *et al.* 2009, Zandt *et al.* 2003). Ward *et al.* (2013) performed a continental scale ambient noise tomography through the Andes and determined for the first time the total extension of the low velocity zones beneath the southern Altiplano and northern Puna. Further joint inversion of surface waves and receiver function revealed the detailed 3D geometry of the Altiplano-Puna Magma Body (Ward *et al.* 2014).

Bianchi *et al.* (2013) carried out a teleseismic P-wave tomography in the southern Puna and detected a low velocity zone in the crust between -26° and -27.5° . They attributed this anomaly to the possible existence of another mid-crustal region with active partial melting, which they referred to as Southern Puna Magma Body (Fig. 1). According to these authors the Altiplano-Puna Magma Body and Southern Puna Magma Body could be disconnected and the limit between both bodies could be

related to the Olacapato-Toro lineament. Calixto *et al.* (2013) reported low crustal velocities between -25° and -27.5° as well, associated with a complex pattern of low and high velocities in the mantle. They interpreted high velocities in the mantle as delaminated blocks and low velocities as hot asthenospheric material responsible for the heating and melting of the crust. Interestingly, anomalous high heat-flow values (> 100 mW/m²) characterize the region; even though reliable data are sparse and scattered, it is still clear that the heat-flow in the plateau is higher than in the surroundings (*e.g.*, Hamza and Muñoz 1996, Henry and Pollack 1988, Springer and Förster 1998). It has been shown that heat conduction alone is not sufficient to account for the observed heat-flow unless high radiogenic heat production values are considered for the crust and extreme heat-flow values are rejected. Otherwise, additional convective and/or advective processes need to be included in order to reproduce high heat-flow (Chapman 1986, Furlong and Chapman 2013).

To the east and north of -23° , in transition to the foreland, the Subandean Ranges are composed of Paleozoic, Mesozoic and Cenozoic sedimentary rocks that form a thin-skinned fold and thrust belt with eastward-younging piggy-back basins (Dunn *et al.* 1995, Mingramm *et al.* 1979). In contrast, south of -23° , the Santa Barbara System consists of Paleozoic rocks with overlying Cretaceous and Cenozoic sedimentary and volcanic rocks associated with the Salta Rift, which was subsequently inverted by compressional tectonics during Andean shortening (Kley and Monaldi 2002, Marquillas *et al.* 2005).

METHODS

The key methodology applied in this study is the calculation of Curie point depth (CDP) and effective elastic thickness (T_e) of the lithosphere. The CDP was calculated from the statistical analysis of the magnetic anomaly in frequency domain (Bhattacharyya and Leu 1977, Okubo *et al.* 1985, Spector and Grant 1970, Tanaka *et al.* 1999). T_e was determined from the analysis of the deflection of the lithosphere and the applied loads in the frequency

domain (Garcia *et al.* 2014, Soler 2015). It should be noted that there are several different methods and models to calculate both CDPs and T_e , therefore our results represent only one of many other possible solutions.

Curie point depth

The magnetic field of the lithosphere results from contrasts in rocks magnetization; which reflect the difference in composition and properties of rocks within the crust (Thebault and Vervelidou 2015). It is considered that the bottom of the magnetic layer represents the surface where the transition between magnetic rocks and non-magnetic rocks occur, either due to a compositional change or an alteration of the magnetic properties of minerals when Curie temperature is reached. Magnetite is the most common magnetic mineral in the lithosphere, however, it is mainly concentrated in the crust and sparse to absent in the mantle; accordingly, the Moho has been proposed as a magnetic boundary (Wasilewski *et al.* 1979).

Furthermore, the modification of magnetic properties as a function of temperature has been largely investigated since the early studies of Pierre Curie in the XIX century. Weiss and Foex (1911) defined the Curie point (also called Curie temperature) as the temperature at which materials lose their ferromagnetic properties. The Curie temperature of magnetite is ~ 575 – 585°C (Hunt *et al.* 2013); given that the typical geothermal gradient for continental regions is $\sim 25^\circ\text{C}/\text{km}$ (Lowell *et al.* 2014) and Moho depths are commonly greater than 25 km, the Curie temperature of magnetite is reached within the crust and consequently, the Curie point depth (CDP) is generally the bottom of the magnetic layer. The method that we used to estimate the depth to the bottom of the magnetic layer (Z_b) relies on the spectral analysis of magnetic anomalies. We followed the approach of Tanaka *et al.* (1999), based on the formulations of Okubo *et al.* (1985) that integrate the centroid method of Bhattacharyya and Leu (1977) and the spectral analysis method of Spector and Grant (1970). The centroid method recognizes that there is no wavelength in which the signal of the bottom of a magnetic body dominates the signal of the top, and pro-

poses an alternative approach for the calculation of Z_b which consist on the determination of the depths to the top (Z_t) and the centroid (Z_o) of the body (Bhattacharyya and Leu 1977, Okubo *et al.* 1985). Since Bhattacharyya and Leu (1977) formulated their method for isolated magnetic anomalies, the integration of the spectral analysis of Spector and Grant (1970) that examines patterns of magnetic anomalies makes it more suitable for regional studies (Tanaka *et al.* 1999). The limitation of the method is that it considers the sources of the anomalies as rectangular vertical prisms, with random magnetization and no remnant component.

A key point of the methodology is the determination of the window size for the calculation of the spectrum because it controls the trade-off between maximum investigation depth and horizontal resolution. Blakely (1996) suggests using windows between 50 and 160 km to cover the whole range of possible Curie point depths, however, more recent studies and model simulations suggest an optimal dimension of about 10 times the investigation depth (Chiozzi *et al.* 2005). Additionally, the application of the "moving window" technique with superposition of windows between consecutive steps prevents the isolation of the signal in each window, working as a low-pass filter that reduces the effect of peaks (Chiozzi *et al.* 2005).

We extracted the magnetic anomaly for the region from the global model EMAG2 (Earth Magnetic Anomaly Grid), compiled from satellite, marine, aeromagnetic and field measurements (Fig. 2; Maus *et al.* 2009). We chose a window size of 200 km by 200 km with a superposition of 50% in both, N-S and E-W directions, resulting in a total number of 64 windows. The depth to the top (Z_t), centroid (Z_o) and bottom (Z_b) of the magnetic source considering a semi-infinite horizontal layer were calculated using the equations as presented by Githiri *et al.* (2012):

$$\ln \left[\frac{P(s)^{1/2}}{|s|} \right] = \ln B - 2\pi|s|Z_t \quad (1)$$

$$\ln \left[\frac{P(s)^{1/2}}{|s|} \right] = \ln A - 2\pi|s|Z_o \quad (2)$$

$$Z_b = 2Z_o - Z_t = CPD \quad (3)$$

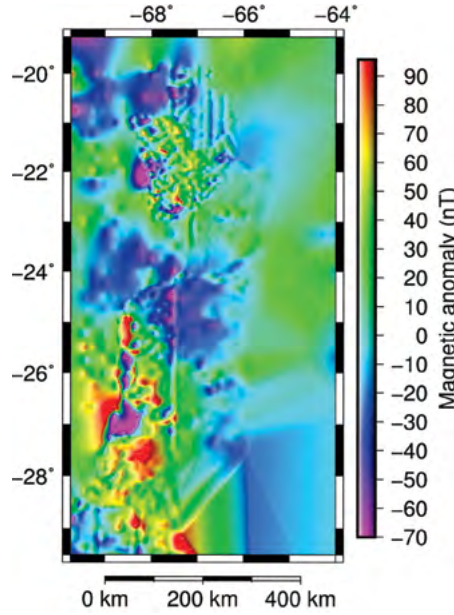


Figure 2. Magnetic anomaly of the region extracted from the global model EMAG2.

where P is the radially averaged power spectrum of the anomaly, s is wavenumber and A and B are constants (Bhattacharyya and Leu 1977, Okubo *et al.* 1985, Spector and Grant 1970).

Finally, using the calculated $CPDs$ we constructed a surface corresponding to the depth of the Curie isotherm (Fig. 3a). The depth is expressed as depth below the topography.

Heat-flow

Following the previous section, the definition of the depth to the bottom of the magnetic sources, interpreted as the depth to the Curie isotherm, provides information on the thermal state of the lithosphere and allows for an estimation of heat-flow. The geothermal gradient (GG) associated with each CPD assuming that heat is transferred solely by conduction was calculated as follows:

$$GG = \frac{T_2 - T_1}{Z_2 - Z_1} \quad (4)$$

where T_2 is Curie temperature (585°C), T_1 is mean annual surface temperature (10°C), Z_2 is Curie point depth and Z_1 is the reference level (0 m).

Assuming a constant thermal conductivity (λ) of 2.5 W/mK (Jaupart and Mareschal,

2011) between the Curie point depth and the surface, we calculated the heat-flow (Q) at the surface (Fig. 3b):

$$Q = GG \cdot \lambda \quad (5)$$

In order to test our results, we compiled surface heat-flow data for the region (Table 1; Hamza and Muñoz 1996, Henry and Pollack 1988, Springer and Förster 1998).

Effective elastic thickness

The elastic thin plate model has been widely used to describe the response of the lithosphere to internal and external loads. According to this model, the lithosphere maintains gravitational equilibrium over long geological time scales by bending over the asthenosphere (Burov and Diament 1995). The following is a simple formulation of the problem relating flexure and topographic loads:

$$D\nabla^4 w(x, y) + (\rho_m - \rho_c)gw(x, y) = \rho_t gh(x, y) \quad (6)$$

where w is deflection, h is topography, g is acceleration of gravity, D is flexural rigidity of the lithosphere, ρ_t is density of the topographic load, ρ_m is density of the mantle and ρ_c is density of the crust.

The flexural rigidity of a lithospheric plate characterizes its resistance to bending moments and depends on the effective elastic thickness of the plate (T_e), the Young modulus (E) and the Poisson ratio (ν):

$$D = \frac{ET_e^3}{12(1-\nu^2)} \quad (7)$$

The effective elastic thickness is usually used to make inferences on the thermal state and strength of the lithosphere. However, it is important to note that the concept of T_e is theoretical and that it represents the thickness of a plate with homogeneous elastic properties (E, ν) (Stüwe 2007).

We calculated the effective elastic thickness modifying the method and Python code of Soler (2015) based on the spectral methods developed by Garcia *et al.* (2014). Equations 6 and 7 provide a good approximation of the method; if the deflection $w(x, y)$, topography $h(x, y)$, densities (ρ_t, ρ_m, ρ_c) and elastic properties (E, ν) are known, then the effective elastic thickness can be calculated.

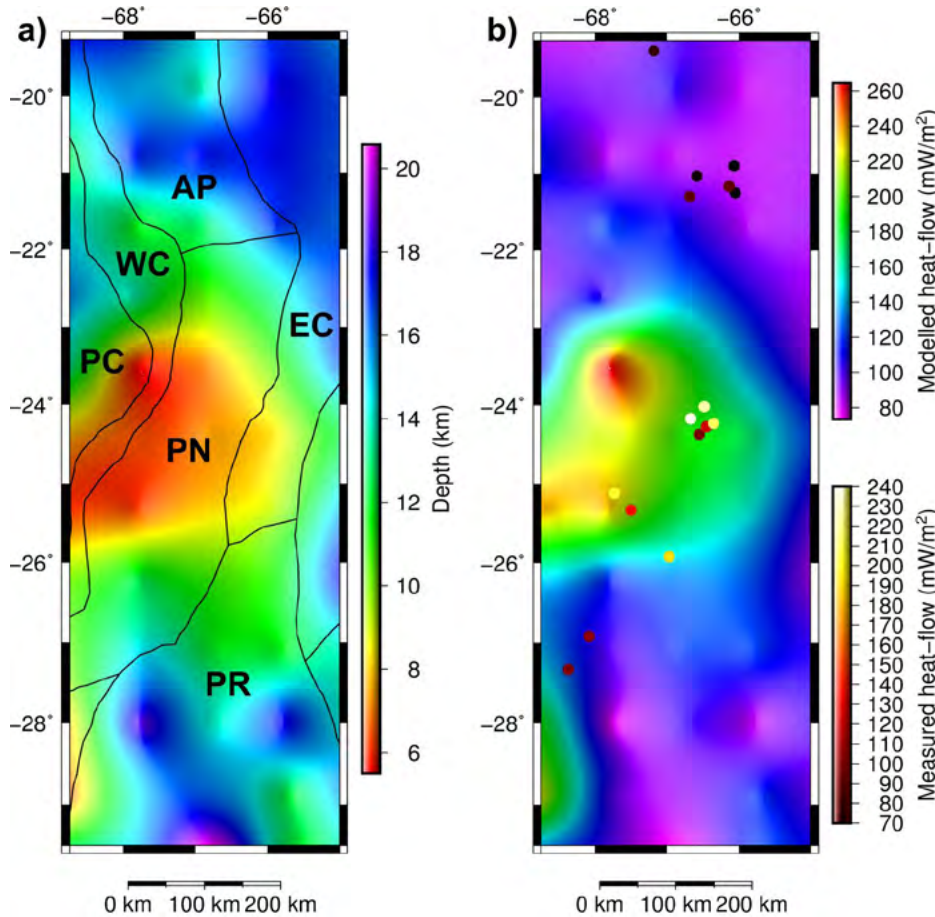


Figure 3. a) Depth to the Curie isotherm with boundaries between morphotectonic units (continuous black lines); b) Calculated heat-flow and color-coded single point data compiled from the literature. AP: Altiplano; PN: Puna; WC: Western Cordillera; PC: Precordillera; EC: Eastern Cordillera; PR: Pampean Ranges.

We assigned average values for the elastic properties of crustal rocks, 100 GPa for the Young modulus (Tesauro *et al.* 2015) and 0.25 for the Poisson ratio (Zandt and Ammon 1995); and we chose densities of 2670 kg/m³, 2850 kg/m³ and 3330 kg/m³ for the topographic load, crust and mantle, respectively (Ibarra *et al.* 2019; Prezzi *et al.* 2009). Finally, the code requires the Bouguer anomaly and the topography as inputs to first invert the gravity anomaly and obtain the deflection, and then calculate the effective elastic thickness.

Given the highly heterogeneous nature of the crust beneath the plateau (e.g., Beck and Zandt 2002, Bianchi *et al.* 2013, Ibarra *et al.* 2019, Prezzi *et al.* 2009, Schurr *et al.* 2003), using a unique average density for the crust to invert the for the Moho and calculate T_e would result in an oversimplification of the problem. Thus, instead of inverting the Bouguer anomaly to define the deflection, we used a crustal thickness

model of South America obtained through compilation of crustal thickness data (from receiver function analysis, seismic refraction experiments and surface-wave dispersion) and interpolation using surface-wave tomography ("Moho B2", Assumpção *et al.* 2013; Fig. 4d).

Furthermore, in order to include the effect of the internal loads that arise from the heterogeneous distribution of density in the crust (Fig. 4b), we calculated a pseudo-topography (Ebbing 2002) from the 3D density model of Ibarra *et al.* (2019) and used it as input for the code instead of the topography. First, the internal load (L) of each body in the model is calculated as the difference between the density of the body and the density of the reference crust (ρ_c) multiplied by the thickness of the body in every X-Y position. Then, the total L of all crustal columns (sum of L of each body at the respective X-Y position) is divided by the density of the topographic load (ρ_t)

to obtain the thickness of a topographic column with an equivalent load. Finally, this thickness is added to the topography to obtain the pseudo-topography:

$$h_{pt} = h + \frac{\sum_{i=1}^N h_i (\rho_i - \rho_c)}{\rho_t} \quad (8)$$

where h_{pt} is the pseudo-topography and h_i and ρ_i are the thickness and density of the each layer in the model of Ibarra *et al.* (2019), respectively.

In order to account for the variations of T_e throughout the region, the code works with small windows (we chose 20 km by 20 km) assuming that T_e is constant in the interior. Several "try-out deflections" are calculated for T_e between 0 km and 50 km for the entire region and then compared against the real deflection (in our case, the seismic Moho) within the window. Finally, the chosen T_e will be the one that minimizes the standard deviation between both deflections ("try-out" and real) in the window (Figure 4c shows the histogram of standard deviations). This T_e is assigned to the center of the window and finally used to interpolate T_e for the entire region (Figure 4a).

RESULTS

Curie depth

Results are limited to the area with available data on the magnetic anomalies in the model EMAG2 (Fig. 2). The depth to the Curie isotherm is relatively shallow throughout the whole region (~5-25 km; Fig. 3a). A zone with depths shallower than 13 km is recognized in the Western Cordillera and Puna plateau, where the active volcanic arc and the Altiplano-Puna Magma Body and Southern Puna Magma Body are located, respectively. Between -23° to -25.5° in the volcanic arc and the Puna, there is a region showing particularly shallow depth to the isotherm with an average depth of ~7 km. Towards the Altiplano (north of -21°), the Pampean Ranges (south of -27°) and the Eastern Cordillera (east of -66°), the isotherm deepens to depths between ~16-23 km. Additionally, there is a small region on the western boundary between -21° and -23.5° where the depth appears to increase to the west reaching ~15 km.

Heat-flow

The calculated heat-flow (Fig. 3b) shows a close correlation with the depth to the Curie isotherm (Figure 3a), regions with high heat-flow coincide with shallow depths to the Curie isotherm and vice versa. In the volcanic arc and the Puna plateau, heat-flow is higher than 100 mW/m^2 , with extreme values higher than 150 mW/m^2 and up to 260 mW/m^2 in most of the volcanic arc and between -23° and -25.5° in the Puna. In the Altiplano, Pampean Ranges and Eastern Cordillera, the heat-flow is reduced to $80\text{--}95 \text{ mW/m}^2$ which is still a high surface heat-flow.

Effective elastic thickness

The calculated effective elastic thickness is in the range $1\text{--}47 \text{ km}$ (Fig. 4a). The general trend is characterized by low T_e in the orogen ($\sim 5\text{--}18 \text{ km}$) and high T_e towards the foreland and forearc ($\sim 30\text{--}45 \text{ km}$). The lowest T_e values ($\sim 2\text{--}10 \text{ km}$) are located in the volcanic arc (Western Cordillera), the southern Puna plateau and the Eastern Cordillera; in the southern Altiplano and northern Puna there is a region with higher T_e ($\sim 12\text{--}20 \text{ km}$). In the Subandean Ranges, T_e rapidly increases from $\sim 18 \text{ km}$ in the west to $\sim 30\text{--}45 \text{ km}$ in the east. Within the Santa Barbara System T_e is lower, showing values of $\sim 15 \text{ km}$. The Pampean Ranges present an irregular pattern with alternation of high and low T_e from west to east.

DISCUSSION

Our results show that the Curie isotherm is shallow below the volcanic arc and the Altiplano-Puna Magma Body and Southern Puna Magma Body, where partial melts occur (Fig. 3a). The shallowest values coincide with the location of the more active volcanoes in the arc (Láscar, Socompa, Lullailaco, La Pacana caldera; Stern 2004) and overlap only partially with the Altiplano-Puna Magma Body and Southern Puna Magma Body. These results are consistent with the magnetotelluric and deep geomagnetic studies of Schwarz *et al.* (1994) and the attenuation tomography of Schurr *et al.* (2003) that show highest conductivities and attenuation in the same region beneath the volcanic arc. These

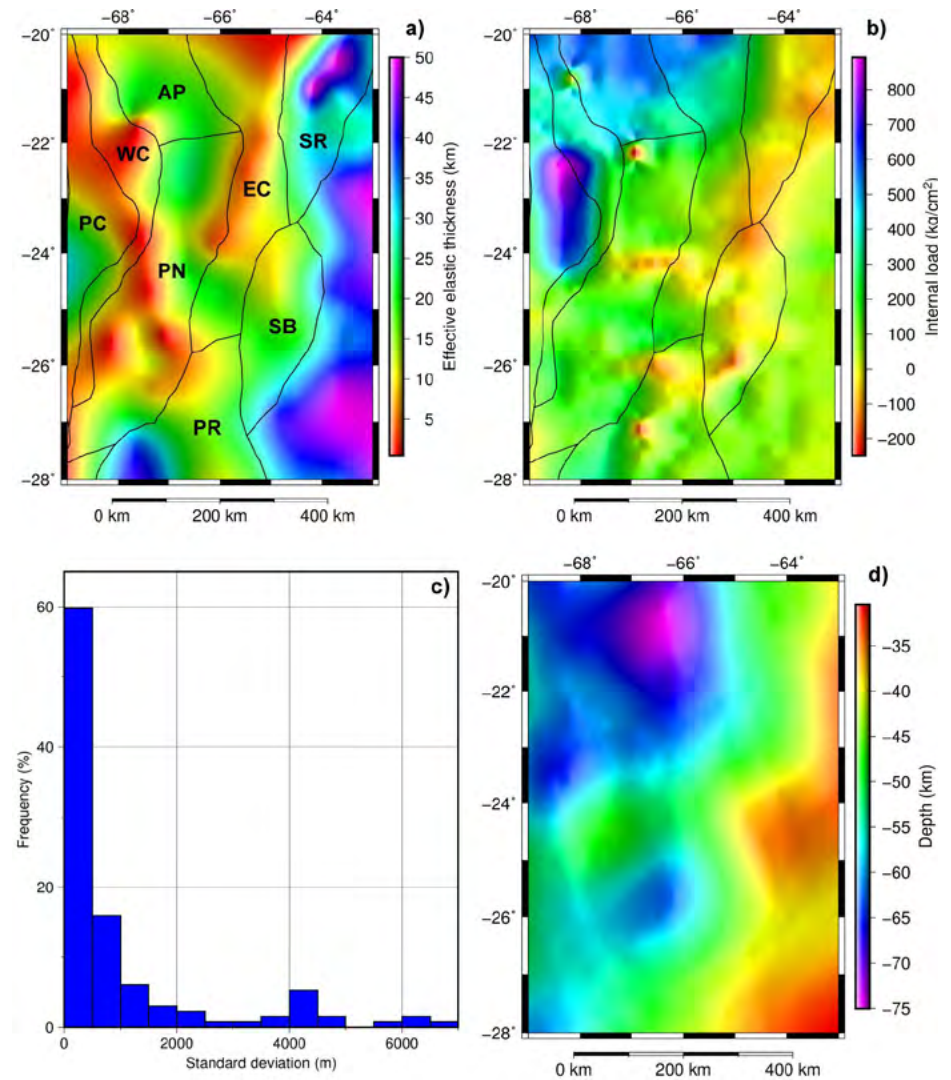


Figure 4. a) Effective elastic thickness with boundaries between morphotectonic units (continuous black lines); b) Internal load calculated from the model of Ibarra *et al.* (2019); c) Histogram of the standard deviation in the calculation of the effective elastic thickness; d) Moho depth taken from the model of Assumpção *et al.* (2013). AP: Altiplano; PN: Puna; WC: Western Cordillera; PC: Precordillera; EC: Eastern Cordillera; PR: Pampean Ranges; SR: Subandean Ranges; SB: Santa Barbara System.

authors suggest that these zones represent pathways for fluid and melt transport; therefore it is likely that given the high temperature of melts and the enhanced transport of heat by convective and advective processes through time, the overall thermal state of the region is altered and the temperatures increased.

The Altiplano presents a deeper Curie isotherm than the Puna, suggesting a difference in the thermal state between both regions. Whitman *et al.* (1996) have already suggested a segmentation of the plateau based on magmatism, topography, tectonics and upper mantle seismic structure. Altogether these observations point to a weaker lithosphere beneath the Puna

which is consistent with higher temperatures and a shallow Curie isotherm. The deeper Curie isotherm below the Pampean Ranges is in agreement with the high P-wave velocities in the region that Bianchi *et al.* (2013) obtained in their teleseismic P-wave tomography. With respect to the small region on the western boundary with increased depth to the Curie isotherm, we observe a partial correlation with the Atacama Block of Schurr and Rietbrock (2004) that was characterized by low attenuation and high P-wave velocities.

Global models of thickness of the magnetic layer show similar results with thicknesses between $10\text{--}25 \text{ km}$ depending on the model (e.g., Li *et al.* 2017, Vervelidou

and Thébault 2015). However, a comparison between our Curie isotherm and the temperature estimates based on geothermometers (e.g., Burns *et al.* 2015, Kay *et al.* 2010) reveals a mismatch of approximately 200°C at 4–8 km. The resolution of our model (100 km) has to be considered as an important error source; due to the limitation of the methodology to provide high resolution when exploring deep sources; we are not able to calculate the Curie depth point for specific locations. Additionally, it has been shown that the method employed in this study works as a low-pass filter, depending on the window size, smoothing the variability of the thermal field and masking local thermal anomalies (Chiozzi *et al.* 2005). On the other hand, the temperatures calculated with geothermometers correspond to the temperature of magmas before eruption and it is expected that the surrounding crust presents lower temperatures. Moreover, geothermometers usually provide uncertainties of 50°C. Considering all these points, we think that the results provide a good approximation to the subsurface temperature distribution.

Regarding heat-flow, the quality of the compiled data is highly variable; some values were obtained through conventional methods while others are estimations based on geochemical methods. The limitations imposed by the sparse and scattered available data are obvious (Fig. 3b); besides, it is difficult to assess the range of uncertainty in the measurements (Hamza *et al.* 2005). However, we observe fairly good coincidence with our results. Table 1 shows that the heat-flow in the southern Altiplano varies between 70 and 94 mW/m² while in the southern Puna oscillates between 100 and 237 mW/m². In Figure 3b there is a clear difference between the southern Altiplano and the Puna, which present values from 80 to 95 mW/m² and 110 to 250 mW/m², respectively. This observation is consistent with the above mentioned segmentation of the plateau, in which the Puna presents higher temperatures and a weaker rheology.

It is worth mentioning that we were able to reproduce high heat-flow values with no consideration of advective and conductive processes and no radiogenic heat production; suggesting that in spite of the

limitations of the method used to calculate the depth to the Curie isotherm, it is a fairly good tool to provide a lower thermal boundary condition for heat-flow calculations.

The calculated effective elastic thickness correlates fairly well with the Curie isotherm (Figs. 3a and 4a). T_e is lower in the Puna plateau and volcanic arc suggesting a higher thermal gradient and weaker lithosphere than the surroundings. However, we have to consider that not always the relation between T_e and temperature is direct and clear; it has been argued that other elements besides the thermal state have an impact on T_e . Burov and Diament (1995) demonstrated with an analytical and numerical approach that T_e can be strongly reduced by crust-mantle decoupling, usually associated with a deep hot Moho, and nonlinear flexure, caused by strong localized deformation. In this region of the Central Andes, the Moho is particularly deep (Assumpção *et al.* 2013) and the deformation is highly localized (Oncken *et al.* 2006), so crust-mantle decoupling and nonlinear flexure have to be considered together with the high temperatures as important mechanisms to explain the extremely reduced T_e values (< 10 km).

The dependence of T_e on multiple factors could explain the less clear segmentation of the plateau between the Altiplano and the Puna regarding T_e . For example, even though temperatures and heat-flow are higher in the Puna suggesting a lower T_e , the Moho is deeper in the Altiplano (Assumpção *et al.* 2013) favoring crust-mantle decoupling and reducing T_e . Further numerical and analytical models need to be carried out in order to better assess the processes behind the observations. In the forearc and foreland, where deformation is scattered and the Moho is shallow, the correlation between temperature and T_e is more direct, suggesting a progressively colder and stronger lithosphere to the west and east of the orogen. However, in the forearc, coupling with the subducting Nazca plate could also be considered as an element controlling T_e .

Interestingly, our results show that T_e is higher in the Subandean Ranges (up to 45 km) than in the Santa Barbara System (up to 20 km). This observation correlates with different styles of deformation between the

Table 1. Compilation of heat-flow data

Latitude	Longitude	Heat-flow (mW/m ²)
-27.33	-68.37	100
-26.92	-68.08	105
-25.92	-66.97	190
-25.33	-67.50	135
-25.12	-67.73	205
-24.37	-66.55	100
-24.27	-66.45	121
-24.23	-66.35	213
-24.17	-66.67	237
-24.02	-66.48	225
-21.30	-66.68	94
-21.25	-66.05	70
-21.17	-66.13	94
-21.03	-66.58	75
-20.90	-66.07	70
-19.38	-67.18	83

morphotectonic units; a thin-skinned system in the Subandean Ranges and thick-skinned deformation in the Santa Barbara System, explained by simple shear and pure shear, respectively (Allmendinger *et al.* 1997).

Watts *et al.* (1995) were the firsts to propose that thin-skinned deformation in the Subandean Ranges is associated with a strong lithosphere presenting high T_e values, whereas thick-skinned deformation in the Santa Barbara System is related to a weak lithosphere with low T_e . Recently, García *et al.* (2018) modelled the effective elastic thickness in the region and obtained high T_e values in the Subandean Ranges (90 km) and low T_e values in the Santa Barbara System (10 km), in agreement with the observations of Watts *et al.* (1995). These authors suggested that T_e is controlled by the thermal state of the lithosphere, given the low heat-flow values in the Subandean Ranges.

Comparing our results, we observe the same trend but different values; our T_e is about half in the Subandean Ranges (45 km) and twice in the Santa Barbara System (20 km). This difference is the result of different Moho depths and loads used to calculate T_e ; for example, in the Subandean Ranges our model presents a deeper Moho and less internal loads which translates into a lower T_e . However, we argue

that in this particular case the thermal state is not controlling the difference in T_e between both regions. Heat-flow data is only available for the Subandean Ranges and, as it was mentioned before, these values have large uncertainties (Hamza *et al.* 2005). Additionally, the blanketing effect of sediments and active thrusting in the Subandean Ranges can reduce surface heat-flow while temperatures in the sub-surface are not necessarily low (Jeffreys 1931, Wangen 1995). On the other hand, seismic studies do not show strong differences in P and S wave velocities (Chulick *et al.* 2013, Feng *et al.* 2004). Therefore, we do not see any strong evidence supporting a significant difference in the thermal state of the Subandean Ranges and the Santa Barbara System that could explain the different T_e . We suggest that other factors such as crust-mantle decoupling and/or nonlinear flexure could explain the observations.

Another possible scenario is that the T_e we observe today in the Santa Barbara System is actually inherited. Watts and Burov (2003) suggested that given the long time scales at which the lithosphere is effectively elastic, the T_e acquired in the last tectonic event is frozen and will slowly change with time. The Santa Barbara System is an inverted late Cretaceous-Paleocene rift (*e.g.*, Kley *et al.* 2005), and rift systems are characterized by particularly low T_e values (Watts and Burov 2003). We propose that during the rift stage, the region weakened and acquired low T_e values which are still characteristic of the Santa Barbara System given the relatively short time elapsed since then.

CONCLUSIONS

We presented new constraints on the temperature distribution beneath the Altiplano-Puna plateau and surrounding regions by assessing the depth to the Curie isotherm based on the inspection of the magnetic anomaly in frequency domain. Furthermore, we calculated the effective elastic thickness of the lithosphere in the region to analyze its relation with thermal state and deformation. We find that:

1. the Curie isotherm is shallow beneath the volcanic arc and the Puna (< 13 km)

where the presence of partial melts within the crust has been proposed based on strong conductivity and velocity anomalies and large ignimbritic deposits;

2. the shallowest depths to the Curie isotherm (< 7 km) are located in the region of the volcanic arc, where the more active volcanoes have been reported and the higher conductivities and attenuations are found, suggesting that convective and/or advective processes in the form of magma and fluids ascending through the crust have enhanced the transport of heat;

3. there is a segmentation in the plateau between the Altiplano and the Puna with respect to Curie depth and heat-flow in agreement with other observations pointing to a weaker lithosphere in the Puna. The Altiplano presents Curie depths around 16-23 km and heat-flow values between 70 and 94 mW/m², whereas beneath the Puna, the depth to the Curie isotherm is less than 13 km and heat-flow values range between 100 and 237 mW/m²;

4. in spite of the limitations of the method, the determination of the Curie isotherm is a good instrument to define lower boundary conditions for heat-flow calculations;

5. the effective elastic thickness is low in the orogen (< 18 km) and high in the forearc and foreland (up to 45 km) correlating with the large scale thermal variability of the lithosphere, as indicated by our Curie isotherm and other geophysical studies;

6. the segmentation between the Altiplano and the Puna is not clear regarding effective elastic thickness. Thus, we suggest that other factors besides temperature, such as crust-mantle decoupling, are controlling the effective elastic thickness;

7. the effective elastic thickness in the Subandean Ranges (45 km) is higher than in the Santa Barbara System (20 km). Since we do not find any strong evidence supporting a significant difference in the thermal state, we suggest that the low effective elastic thickness in the Santa Barbara System is inherited from the previous Cretaceous-Paleocene rifting in the region.

We emphasize that correlations between T_e and thermal state and strength of the continental lithosphere need to be carefully evaluated in the light of different factors and/or compared against other calcula-

tions based on temperature estimates and rock properties.

ACKNOWLEDGEMENTS

This research was funded by CONICET (Consejo Nacional de Investigaciones Científicas y Técnicas) within the framework of the International Research Group "SuRfAce processes, TEctonics and Georesources: The Andean foreland basin of Argentina" (GII 739 StRATEGy).

All the figures were plotted with GMT (Wessel *et al.* 2013). We gratefully thank the editor and three anonymous reviewers for their contribution to improve the manuscript.

REFERENCES

- Allmendinger, R. W., Jordan, T. E., Kay, S. M., and Isacks, B. L. 1997. The Evolution of the Altiplano-Puna Plateau of the Central Andes. *Annual Review of Earth and Planetary Sciences* 25(1): 139-174.
- Alonso, R. N., Jordan, K., Tabutt, K., and Vandervort, D. 1991. Giant Evaporite Belts in the Neogene Central Andes. *Geology* 19: 401-404.
- Assumpção, M., Feng, M., Tassara, A., and Juliã, J. 2013. Models of crustal thickness for South America from seismic refraction, receiver functions and surface wave tomography. *Tectonophysics* 609: 82-96.
- Babeyko, A. Y., Sobolev, S. V., Trumbull, R. B., Oncken, O., and Lavier, L. L. 2002. Numerical models of crustal scale convection and partial melting beneath the Altiplano-Puna plateau. *Earth and Planetary Science Letters* 199(3-4): 373-388.
- Beck, S. L., and Zandt, G. 2002. The nature of orogenic crust in the central Andes. *Journal of Geophysical Research: Solid Earth* 107(B10): 2230.
- Bhattacharyya, B. K., and Leu, L. K. 1977. Spectral analysis of gravity and magnetic anomalies due to rectangular prismatic bodies. *Geophysics* 42(1): 41-50.
- Bianchi, M., Heit, B., Jakovlev, A., Yuan, X., Kay, S. M., Sandvol, E., Alonso, R. N., Coira, B., Brown, L., Kind, R., & Comte, D. 2013. Teleseismic tomography of the southern Puna plateau in Argentina and adjacent regions. *Tectonophysics* 586: 65-83.
- Blakely, R. J. 1996. *Potential Theory in Gravity and Magnetic Applications*. Cambridge University Press, 441 p., Cambridge.

- Brasse, H., Lezaeta, P., Rath, V., Schwalenberg, K., Soyer, W., and Haak, V. 2002. The Bolivian Altiplano conductivity anomaly. *Journal of Geophysical Research* 107(B5): 2096.
- Burns, D. H., de Silva, S. L., Tepley, F., Schmitt, A. K., and Loewen, M. W. 2015. Recording the transition from flare-up to steady-state arc magmatism at the Purico-Chascon volcanic complex, northern Chile. *Earth and Planetary Science Letters* 422: 75-86.
- Burov, E. B., and Diament, M. 1995. The effective elastic thickness (T_e) of continental lithosphere: what does it really mean? *Journal of Geophysical Research* 100(B3): 3905-3927.
- Calixto, F. J., Sandvol, E., Kay, S., Mulcahy, P., Heit, B., Yuan, X., Coira, B., Comte, D., & Alvarado, P. 2013. Velocity structure beneath the southern Puna plateau: Evidence for delamination. *Geochemistry, Geophysics, Geosystems* 14(10): 4292-4305.
- Chapman, D. S. 1986. Thermal gradients in the continental crust. In: Dawson, J.M., Carswell, D. A., Hall, J. and Wedepohl, K.H. (eds.) *The Nature of the Lower Continental Crust*. The Geological Society, p. 63-70, London.
- Chiozzi, P., Matsushima, J., Okubo, Y., Pasquale, V., and Verdoya, M. 2005. Curie-point depth from spectral analysis of magnetic data in central – southern Europe. *Physics of the Earth and Planetary Interiors* 152: 267-276.
- Chmielowski, J., Zandt, G., and Haberland, C. 1999. The Central Andean Altiplano-Puna Magma Body. *Geophysical Research Letters* 26(6): 783-786.
- Chulick, G. S., Detweiler, S., and Mooney, W. D. 2013. Seismic structure of the crust and uppermost mantle of South America and surrounding oceanic basins. *Journal of South American Earth Sciences* 42: 260-276.
- Coira, B., and Kay, S. M. 1993. Implications of Quaternary volcanism at Cerro Tuzgle for crustal and mantle evolution of the high Puna Plateau, Central Andes, Argentina. *Contributions to Mineralogy and Petrology* 113: 40-58.
- Comeau, M. J., Unsworth, M. J., and Cordell, D. 2016. New constraints on the magma distribution and composition beneath Volcán Uturuncu and the southern Bolivian Altiplano from magnetotelluric data. *Geosphere* 12(5): 1391-1421.
- Comeau, M. J., Unsworth, M. J., Ticona, F., and Sunagua, M. 2015. Magnetotelluric images of magma distribution beneath Volcán Uturuncu, Bolivia: Implications for magma dynamics. *Geology* 43(3): 243-246.
- de Silva, S. 1989. Altiplano-Puna volcanic complex of the Central Andes. *Geology* 17: 1102-1106.
- Díaz, D., Brasse, H., and Ticona, F. 2012. Conductivity distribution beneath Lascar volcano (Northern Chile) and the Puna, inferred from magnetotelluric data. *Journal of Volcanology and Geothermal Research* 217-218: 21-29.
- Dunn, J. F., Hartshorn, K. G., and Hartshorn, P. W. 1995. Structural styles and hydrocarbon potential of the Subandean thrust belt of Southern Bolivia. In: Tankard, A.J., Suarez Soruco, R., and Welsink, H.J. (eds.), *Petroleum Basins of South America*. AAPG Memoir 62: 523-543.
- Ebbing, J. 2002. 3-D Dichteverteilung und isostatisches Verhalten der Lithosphäre in den Ostalpen. PhD Thesis (Unpublished), Freie Universität Berlin, 143 p., Berlin.
- Feng, M., Assumpção, M., and Van der Lee, S. 2004. Group-velocity tomography and lithospheric S-velocity structure of the South American continent. *Physics of the Earth and Planetary Interiors* 147(4): 315-331.
- Furlong, K. P., and Chapman, D. S. 2013. Heat Flow, Heat Generation, and the Thermal State of the Lithosphere. *Annual Review of Earth and Planetary Sciences* 41: 385-410.
- García, E. S., Sandwell, D. T., and Luttrell, K. M. 2014. An iterative spectral solution method for thin elastic plate flexure with variable rigidity. *Geophysical Journal International* 200(2): 1012-1028.
- García, H. P. A., Gianni, G. M., Lupari, M. N., Sánchez, M. A., Soler, S. R., Ruiz, F., and Lince Klinger, F. G. 2018. Effective elastic thickness in the Central Andes. Correlation to orogenic deformation styles and lower crust high-gravity anomaly. *Journal of South American Earth Sciences* 87: 232-246.
- Githiri, J. G., Patel, J. P., Barongo, J. O., and Karanja, P. K. 2012. Spectral analysis of ground magnetic data in Magadi area, southern Kenya rift. *Tanzania Journal of Science* 38(1): 1-14.
- Guzmán, S., Grosse, P., Montero-López, C., Hongn, F., Pilger, R., Petrinovic, I., Seggiaro, R., & Aramayo, A. 2014. Spatial-temporal distribution of explosive volcanism in the 25-28°S segment of the Andean Central Volcanic Zone. *Tectonophysics* 636: 170-189.
- Hamza, V. M., Dias, F. J. S. S., Gomes, A. J. L., and Terceros, Z. G. D. 2005. Numerical and functional representations of regional heat flow in South America. *Physics of the Earth and Planetary Interiors* 152(4): 223-256.
- Hamza, V. M., and Muñoz, M. 1996. Heat flow map of South America. *Geothermics* 25(6): 599-646.
- Henry, S., and Pollack, H. 1988. Terrestrial Heat Flow Above the Andean Subduction Zone in Bolivia and Peru. *Journal of Geophysical Research* 93(B12): 153-162.
- Hunt, C. P., Moskowitz, B. M., and Banerjee, S. K. 2013. Magnetic Properties of Rocks and Minerals. In: T. J. Ahrens (ed.), *Rock Physics and Phase Relations*. AGU Reference Shelf, 189-204, Washington D. C.
- Ibarra, F., Liu, S., Meeßen, C., Prezzi, C. B., Bott, J., Scheck-Wenderoth M., Sobolev, S., and Strecker, M. R. 2019. 3D data-derived lithospheric structure of the Central Andes and its implications for deformation: insights from gravity and geodynamic modelling. *Tectonophysics* 766: 453-468.
- Isacks, B. L. 1988. Uplift of the Central Andean Plateau and Bending of the Bolivian Orocline. *Journal of Geophysical Research* 93: 3211-3231.
- Jaupart, C., and Mareschal, J. C. 2011. *Heat generation and transport in the Earth*. Cambridge University Press, 646 p., Cambridge.
- Jeffreys, H. 1931. The Thermal Effects of Blanketing by Sediments. *Geophysical Supplements to the Monthly Notices of the Royal Astronomical Society* 2(7): 323-329.
- Jordan, T. E., Isacks, B. L., Allmendinger, R. W., Brewer, J., Ramos, V. A., and Ando, C. 1983. Andean tectonics related to geometry of the subducted Nazca plate. *Geological Society of America Bulletin* 94: 341-361.
- Kay, S. M., Coira, B., and Viramonte, J. 1994. Young mafic back arc volcanic rocks as indicators of continental lithospheric delamination beneath the Argentine Puna Plateau, Central Andes. *Journal of Geophysical Research* 99: 24323-24339.
- Kay, Suzanne Mahlburg, Coira, B. L., Caffè, P. J., and Chen, C. H. 2010. Regional chemical diversity, crustal and mantle sources and evolution of central Andean Puna plateau ignimbrites. *Journal of Volcanology and Geothermal Research* 198(1-2): 81-111.
- Kley, J., and Monaldi, C.R. 2002. Tectonic inversion in the Santa Bárbara System of the central Andean foreland thrust belt, north-western Argentina. *Tectonics* 21: 1061-1079.

- Kley, J., Rossello, E.A., Monaldi, C. R., and Habighorst, B. 2005. Seismic and field evidence for selective inversion of Cretaceous normal faults, Salta rift, northwest Argentina. *Tectonophysics* 399(1-4 SPEC. ISS.): 155-172.
- Koulakov, I., Sobolev, S.V., and Asch, G. 2006. P - And S-velocity images of the lithosphere-asthenosphere system in the Central Andes from local-source tomographic inversion. *Geophysical Journal International* 167(1): 106-126.
- Lamb, S. 2000. Active deformation in the Bolivian Andes, South America. *Journal of Geophysical Research* 105: 2627-2653.
- Li, C.F., Lu, Y., and Wang, J. 2017. A global reference model of Curie-point depths based on EMAG2. *Scientific Reports* 7(2): 1-9.
- Lowell, R. P., Koldaivelu, K., and Rona, P. A. 2014. Hydrothermal Activity. Reference Module in Earth Systems and Environmental Sciences (3): 1-19.
- Marquillas, R. A., del Papa, C., and Sabino, I. F. 2005. Sedimentary aspects and paleoenvironmental evolution of a rift basin: Salta Group (Cretaceous-Paleogene), northwestern Argentina. *International Journal of Earth Sciences* 94: 94-113.
- Maus, S., Barckhausen, U., Berkenbosch, H., Bournas, N., Brozena, J., Childers, V., Dostal, F., Fairhead, J., Finn, C., von Frese, R., Gaina, C., Golynsky, S., Kucks, R., Lühr, H., Milligan, P., Mogren, S., Müller, R., Olesen, O., Pilkington, M., Saltus, R., Schreckenberger, B., Thébaud, E., and Caratori Tontini, F. 2009. EMAG2: A 2-arc min resolution Earth Magnetic Anomaly Grid compiled from satellite, airborne, and marine magnetic measurements. *Geochemistry Geophysics Geosystems* 10(8): Q08005.
- Mantovani, M. S., Shukowsky, W., de Freitas, S. R., and Neves, B. B. 2005. Lithosphere mechanical behavior inferred from tidal gravity anomalies: a comparison of Africa and South America. *Earth and Planetary Science Letters* 230: 397-412.
- Mingramm, A., Russo, A., Pozzo, A., and Cazau, L. 1979. Sierras Subandinas. In: J. C. M. Turner (ed.), *Geología Regional Argentina*. Academia Nacional de Ciencias, Volumen 1: 95-138.
- Okubo, Y., Graf, R. J., Hansen, R. O., Ogawa, K., and Tsu, H. 1985. Curie point depths of the Island of Kyushu and surrounding areas, Japan. *Geophysics* 50(3): 481-494.
- Oncken, O., Hindle, D., Kley, J., Elger, K., Victor, P., and Schemmann, K. 2006. Deformation of the central Andean upper plate system-Facts, fiction, and constraints for plateau models. In: Oncken, O., Chong, G., Franz, G., Giese, P., Götze, H.J., Ramos, V.A., Strecker, M.R. and Wigger, P. (eds.), *The Andes: Active Subduction Orogeny* (pp. 3-27). Springer-Verlag, *Frontiers in Earth Science Series*, Berlin
- Ouimet, W. B., and Cook, K. L. 2010. Building the central Andes through axial lower crustal flow. *Tectonics* 29(3): 1-15.
- Pérez-Gussinyé, M., Swain, C., Kirby, J., and Lowry, A. 2009. Spatial variations of the effective elastic thickness, T_e , using multitaper spectral estimation and wavelet methods: Examples from synthetic data and application to South America. *Geochemistry, Geophysics, Geosystems* 10(4): Q04005
- Prezzi, C. B., and Ibarra, F. 2017. Estructura cortical del noroeste de Argentina a partir de datos gravimétricos y magnetométricos. In: Muruaga, C.M. and Grosse, P. (eds.) *Ciencias de la Tierra y Recursos Naturales del NOA*. Asociación Geológica Argentina, 54-69, San Miguel de Tucumán.
- Prezzi, C. B., Götze, H. J., and Schmidt, S. 2009. 3D density model of the Central Andes. *Physics of the Earth and Planetary Interiors* 177(3-4): 217-234.
- Prezzi, C., Iglesia Llanos, M. P., Götze, H. J., and Schmidt, S. 2014. Thermal and geodynamic contributions to the elevation of the Altiplano-Puna plateau. *Physics of the Earth and Planetary Interiors* 237: 51-64.
- Risse, A., Trumbull, R. B., Kay, S. M., Coira, B., and Romer, R. L. 2013. Multi-stage evolution of late neogene mantle-derived magmas from the central andes back-arc in the southern Puna plateau of Argentina. *Journal of Petrology* 54(10): 1963-1995.
- Schmitt, A., de Silva, S., Trumbull, R., and Emmermann, R. 2001. Magma evolution in the Purico ignimbrite complex, northern Chile: evidence for zoning of a dacitic magma by injection of rhyolitic melts following mafic recharge. *Contributions to Mineralogy and Petrology* 140: 680-700.
- Schurr, B., Asch, G., Rietbrock, A., Trumbull, R., and Haberland, C. 2003. Complex patterns of fluid and melt transport in the central Andean subduction zone revealed by attenuation tomography. *Earth and Planetary Science Letters* 215(1-2): 105-119.
- Schurr, B., and Rietbrock, A. 2004. Deep seismic structure of the Atacama basin, northern Chile. *Geophysical Research Letters* 31(12): 10-13.
- Schwarz, G., Diaz, G. C., Krüger, D., Martinez, E., Massow, W., Rath, V., and Viramonte, J. 1994. Crustal High Conductivity Zones in the Southern Central Andes. In: Reutter, K.J., Scheuber, E. and Wigger, P. (eds.), *Tectonics of the Southern Central Andes*. Springer, 49-67, Berlin.
- Siks, B. C., and Horton, B. K. 2011. Growth and fragmentation of the Andean foreland basin during eastward advance of fold-thrust deformation, Puna plateau and Eastern Cordillera, northern Argentina. *Tectonics* 30(6): 1-27.
- Soler, S. 2015. Métodos Espectrales para la Determinación de la Profundidad del Punto de Curie y el Espesor Elástico de la Corteza Terrestre. Tesina de Grado. Universidad Nacional de Rosario.
- Spector, A., and Grant, F. S. 1970. Statistical Models for Interpreting Aeromagnetic Data. *Geophysics* 35(2): 293.
- Springer, M. 1999. Interpretation of heat-flow density in the Central Andes. *Tectonophysics* 306(3-4): 377-395.
- Springer, M., and Förster, A. 1998. Heat-flow density across the central Andean subduction zone. *Tectonophysics* 291(1-4): 123-139.
- Stern, C. R. 2004. Active Andean volcanism: its geologic and tectonic setting. *Revista Geológica de Chile* 31(2): 161-206.
- Stewart, J., and Watts, A. 1997. Gravity anomalies and spatial variations of flexural rigidity at mountain ranges. *Journal of Geophysical Research: Solid Earth* 102: 5327-5352.
- Stüwe, K. 2007. *Geodynamics of the Lithosphere*. An Introduction. Springer-Verlag, 493 p., Berlin Heidelberg.
- Tanaka, A., Okubo, Y., and Matsubayashi, O. 1999. Curie point depth based on spectrum analysis of the magnetic anomaly data in East and Southeast Asia. *Tectonophysics* 306(3-4): 461-470.
- Tassara, A. 2005. Interaction between the Nazca and South American plates and formation of the Altiplano-Puna plateau: Review of a flexural analysis along the Andean margin (15° 34° S). *Tectonophysics* 399: 39-57.
- Tesauero, M., Kaban, M. K., and Mooney, W. D. 2015. Variations of the lithospheric strength and elastic thickness in North America. *Geochemistry Geophysics Geosystems* 16(7): 2197-2220.
- Thebaud, E., and Vervelidou, F. 2015. A statis-

- tical spatial power spectrum of the Earth's lithospheric magnetic field. *Geophysical Journal International* 201(2): 605-620.
- Vervelidou, F., and Thébault, E. 2015. Global maps of the magnetic thickness and magnetization of the Earth's lithosphere. *Earth, Planets and Space* 67(1): 173.
- Viramonte, J. G., Galliski, M. A., Araña Saavedra, V., Aparicio, A., Garcia Cacho, L., and Martín Escorza, C. 1984. El finivolcanismo básico de la depresión de Arizaro, provincia de Salta. IX Congreso Geológico Argentino, Actas 1: 234-251, San Carlos de Bariloche.
- Wangen, M. 1995. The blanketing effect in sedimentary basins. *Basin Research* 7: 283-298.
- Ward, K. M., Porter, R. C., Zandt, G., Beck, S. L., Wagner, L. S., Minaya, E., and Tavera, H. 2013. Ambient noise tomography across the Central Andes. *Geophysical Journal International* 194(3): 1559-1573.
- Ward, K. M., Zandt, G., Beck, S. L., Christensen, D. H., and McFarlin, H. 2014. Seismic imaging of the magmatic underpinnings beneath the Altiplano-Puna volcanic complex from the joint inversion of surface wave dispersion and receiver functions. *Earth and Planetary Science Letters* 404: 43-53.
- Wasilewski, P. J., Thomas, H. H., and Mayhew, M. A. 1979. The Moho as a magnetic boundary. *Geophysical Research Letters* 6(7): 541-544.
- Watts, A. B., and Burov, E. B. 2003. Lithospheric strength and its relationship to the elastic and seismogenic layer thickness 213: 113-131.
- Watts, A., Lamb, S., Fairhead, J., and Dewey, J. 1995. Lithospheric flexure and bending of the Central Andes. *Earth and Planetary Science Letters* 134: 9-21.
- Weiss, P., and Foex, G. 1911. Étude de l'aimantation des corps ferromagnétiques au-dessus du point de Curie. *Journal de Physique Théorique et Appliquée* 1(1): 274-287.
- Wessel, P., Smith, W. H. F., Scharroo, R., Luis, J., and Wobbe, F. 2013. Generic Mapping Tools: Improved Version Released. *Eos, Transactions American Geophysical Union* 94(45): 409-410.
- Whitman, D., Isacks, B. L., and Kay, S. M. 1996. Lithospheric structure and along-strike segmentation of the Central Andean Plateau: seismic Q, magmatism, flexure, topography and tectonics. *Tectonophysics* 259: 29-40.
- Wienecke, S., Braitenberg, C., and Götze, H. J. 2007. A new analytical solution estimating the flexural rigidity in the Central Andes. *Geophysical Journal International* 169: 789-794.
- Wölbern, I., Heit, B., Yuan, X., Asch, G., Kind, R., Viramonte, J., Tawackoli, S., & Wilke, H. 2009. Receiver function images from the Moho and the slab beneath the Altiplano and Puna plateaus in the Central Andes. *Geophysical Journal International* 177(1): 296-308.
- Yuan, X., Sobolev, S. V., Kind, R., Oncken, O., Bock, G., Asch, G., Schurr, B., Graeber, F., Rudloff, A., Hanka, W., Wylegalla, K., Tibi, R., Haberland, Ch., Rietbrock, A., Giese, P., Wigger, P., Röwer, P., Zandt, G., Beck, S., Wallace, T., Pardo, M., & Comte, D. 2000. Subduction and collision processes in the Central Andes constrained by converted seismic phases. *Nature* 408(6815): 958-961.
- Zandt, G., and Ammon, C. J. 1995. Continental crust composition constrained by measurements of crustal Poisson's ratio. *Nature* 374: 152-154.
- Zandt, George, Leidig, M., Chmielowski, J., Baumont, D., and Yuan, X. 2003. Seismic detection and characterization of the Altiplano-Puna magma body, Central Andes. *Pure and Applied Geophysics* 160: 789-807.